https://doi.org/10.5194/tc-2022-182
Preprint. Discussion started: 20 September 2022

The Cryosphere Discussions

Observed and modeled moulin heads in the Pâkitsoq region of Greenland suggest subglacial channel network effects

Celia Trunz[1,2], Kristin Poinar[3], Lauren C. Andrews[4], Matthew D. Covington[1], Jessica Mejia[3,5], Jason Gulley[5], and Victoria Siegel[6]

[1]Geosciences Department, University of Arkansas, Fayetteville AR, USA
[2]Department of Applied Geomatics, Université de Sherbrooke, Sherbrooke, QC, CA
[3]Department of Geology, University at Buffalo, Buffalo NY, USA
[4]Global Modeling and Assimilation Office, NASA Goddard Space Flight Center, Greenbelt MD, USA
[5]Geosciences Department, University of South Florida, Tampa FL, USA
[6]Sisu Field Solutions LLC, Austin, Texas, USA

Correspondence: Celia Trunz (celia.trunz@gmail.com)

Abstract.

In the ablation zone of land-terminating areas of the Greenland Ice Sheet, water pressures at the bed control seasonal and daily ice motion variability. During the melt season, large amounts of surface meltwater access the bed through moulins, which sustain an efficient channelized subglacial system. Water pressure within these subglacial channels can be inferred by measuring the hydraulic head within moulins. However, moulin head data are rare, and subglacial hydrology models that simulate water pressure fluctuations require water storage in moulins or subglacial channels. Neither the volume nor the location of such water storage is currently well constrained. Here, we use the Moulin Shape (MouSh) model, which quantifies time-evolving englacial storage, coupled with a subglacial channel model to simulate head measurements from a moulin in the Pâkitosq region in Greenland. We force the model with surface meltwater input calculated using field-acquired weather data. Our first-order simulations of moulin hydraulic head either over-predict the diurnal range of oscillation of the moulin head or require an unrealistically large moulin size to produce realistic head oscillation ranges. We find that to accurately match field observations of moulin head, additional subglacial water must be added to the system. We hypothesize that this additional 'baseflow' represents strong subglacial network connectivity throughout the channelized system and is ultimately sourced from basal melt and non-local surface water inputs upstream.

1 Introduction

The Greenland Ice Sheet is experiencing increased mass loss via surface melting and calving in response to climatic warming (Hanna et al., 2020). In the ablation zone, most of the seasonal surface melt is routed through supraglacial streams that (Yang and Smith, 2016; Pitcher and Smith, 2019) drains through moulins (Smith et al., 2015), vertical shafts that penetrate the full thickness of the ice sheet. It has been shown that spatial (Banwell et al., 2016) and temporal (Schoof, 2010) supraglacial meltwater input variability can accelerate or decelerate ice flow. The amount, position, and timing of meltwater infiltration into moulins and crevasses determine local and regional ice motion, which in turn affects global sea-level change (Nienow et al., 2017).

The subglacial drainage system is thought to be composed of interspersed efficient and inefficient components (Iken et al., 1996; Mair et al., 2002; Röthlisberger, 1972; Walder, 1986). The efficient system is composed of low-pressure, high-flux subglacial channels, whereas the inefficient system is composed of a network of poorly connected, high-pressure cavities that conduct water at much slower speeds. As the melt season proceeds, the efficient channelized system grows in scope and can increase the connectivity of high-pressure cavities within the inefficient system, conducting water more efficiently overall and slowing ice motion (Andrews et al., 2014; Downs et al., 2018).

Diurnal ice motion cycles during the melt season are mainly influenced by the capacity of the channel-based efficient drainage to accommodate fluctuations in meltwater inputs (Bartholomew et al., 2012; Willis, 1995). Meltwater inputs to moulins initiate and sustain the growth of these subglacial channels, while the ice pressure drives creep closure when meltwater inputs reduce (Schoof, 2010). Moulins directly feed these channels (Catania and Neumann, 2010; Yang and Smith, 2016); consequently, moulin hydraulic head (water column above a datum) reflects the water pressure in the local subglacial channel (Andrews et al., 2014). Despite their utility, field measurements of moulin hydraulic head fluctuations are sparse in Greenland (Andrews et al., 2014; Covington et al., 2020; Cowton et al., 2013; Mejia et al., 2021) and alpine glaciers (Iken, 1972; Badino and Piccini, 2002). This is due to the constraints of field logistics and the technical finesse required to instrument the complex, imperfectly vertical geometry that characterizes moulins (Covington et al., 2020; Gulley et al., 2009). Models for moulin heads are therefore needed if we are to understand diurnal water pressure variations across larger areas of the Greenland Ice Sheet in order to predict how meltwater infiltration affects ice motion (Trunz et al., 2022).

The most advanced subglacial hydrology models currently in wide use are two-dimensional models that simulate water pressure at any grid point as a continuum or a binary choice between two possible subglacial conditions : channels or cavities (e.g., Schoof et al., 2012; Sommers et al., 2018; de Fleurian et al., 2016). This type of model focuses primarily on pressures across the bed. Other two-dimensional models simulate only the channelized drainage system (e.g., Banwell et al., 2013). These two-dimensional models generally require a large number of parameters that often are unknown or uncertain. Alternatively, simpler physically based models have frequently been used to simulate water pressure in subglacial channels (Röthlisberger, 1972), with a subglacial channel that can melt open and creep closed (Spring and Hutter, 1981; Schoof, 2010), and is connected to cavities (Schoof, 2010; Bartholomew et al., 2012) or is not connected to cavities (Covington et al., 2012; Bartholomew et al., 2012; Cowton et al., 2016; Meierbachtol et al., 2013).

Some zero and one-dimensional models couple the subglacial channel to englacial storage via a cylindrical or conical moulin whose shape is static in time (Werder et al., 2013; Covington et al., 2012, 2020; Cowton et al., 2016; Bartholomew et al., 2012; Trunz et al., 2022), but not all models include such storage (de Fleurian et al., 2016). The size and shape of a moulin within the range of its water level oscillations affect the amplitude and temporal pattern of diurnal water pressure oscillations (Werder et al., 2010; Trunz et al., 2022). When these subglacial models are driven by realistic surface meltwater inputs, large englacial or subglacial storage volumes are required in order to produce realistic moulin head outputs (Hoffman et al., 2016; Bartholomew et al., 2012; Covington et al., 2020). To date, the true nature and location of these storage volumes have remained vague or

https://doi.org/10.5194/tc-2022-182
Preprint. Discussion started: 20 September 2022

the object of speculation (Flowers, 2018). For these reasons, we are motivated to investigate the size, shape, and water storage capacity of moulins, how these quantities change over time, and how these parameters affect subglacial water pressure and, therefore, moulin head variability.

In this study, we investigate the hydrodynamics in the englacial-subglacial system using a single-conduit subglacial model coupled with the Moulin Shape (MouSh) englacial hydrology model, which allows the moulin to evolve in size, shape, and storage capacity in response to continued meltwater inputs. We compare modeled hydraulic head fluctuations with field measurements to infer characteristics of the englacial and subglacial systems.

2 Field site

As part of the Moulin Velocity Experiment (MoVE) project (Covington et al., 2020; Mejia et al., 2021), we collected moulin hydraulic head and supraglacial stream discharge measurements just upstream of an instrumented moulin during the 2017 melt season. The moulin was located at 69.4741°N, 49.8232°W, near “Low Camp" (Fig. 1a–b) in the Pâkitsoq region of the Greenland Ice Sheet. The site is approximately 25 km from the ice sheet margin at 780 $\mathrm{m.a.s.l.}$ where the ice is approximately 500 m thick (Morlighem et al., 2017). For simplicity, throughout the text we refer to these field features as the “moulin” and its “stream”.

We collected moulin water levels every 15 minutes between July to October 2017 (Mejia et al., 2020b), however, we only use the moulin hydraulic head for a 40-day period during the melt season from mid-July through August 2017, after which surface meltwater input ceased. To ensure that the model and the measurements have the same point of reference, we use the bed at the moulin as the datum (we place the bed at 0 m), and we convert water pressure measurements to hydraulic head using the BedMachine-derived bed elevation and ice thickness (Morlighem et al., 2017) at the moulin site.

3 Model and methods

We simulate the size, shape, and hydraulic head of a moulin instrumented in the field using the Moulin Shape (MouSh) model (Andrews et al., 2022) coupled to a subglacial channel model (Covington et al., 2020) based on the Schoof (2010) equations for melt and creep closure.

All the components of the coupled moulin–subglacial channel model are illustrated in Figure 2. We force the model with varying surface input with an amplitude (A_{in}) and mean discharge ($\overline{Q}_{\mathrm{in}}$), which induces head ($h$) oscillations around the equilibrium head (h_{eq}) with an amplitude of oscillation (A_{h}). The water storage in the moulin is controlled by the co-evolution of the moulin radius (r_m) and the subglacial channel radius (r_{sc}). We also input a subglacial baseflow term (Q_{bf}) which prescribes the amount of water flowing in the subglacial channel without directly specifying flow or melt within the moulin. This baseflow can either be held constant or allowed to oscillate around a mean value ($\overline{Q}_{\mathrm{bf}}$) with a peak-to-peak amplitude (A_{bf}), as qualitatively illustrated in Fig. 2.

https://doi.org/10.5194/tc-2022-182
Preprint. Discussion started: 20 September 2022

The Cryosphere
Discussions
Open Access

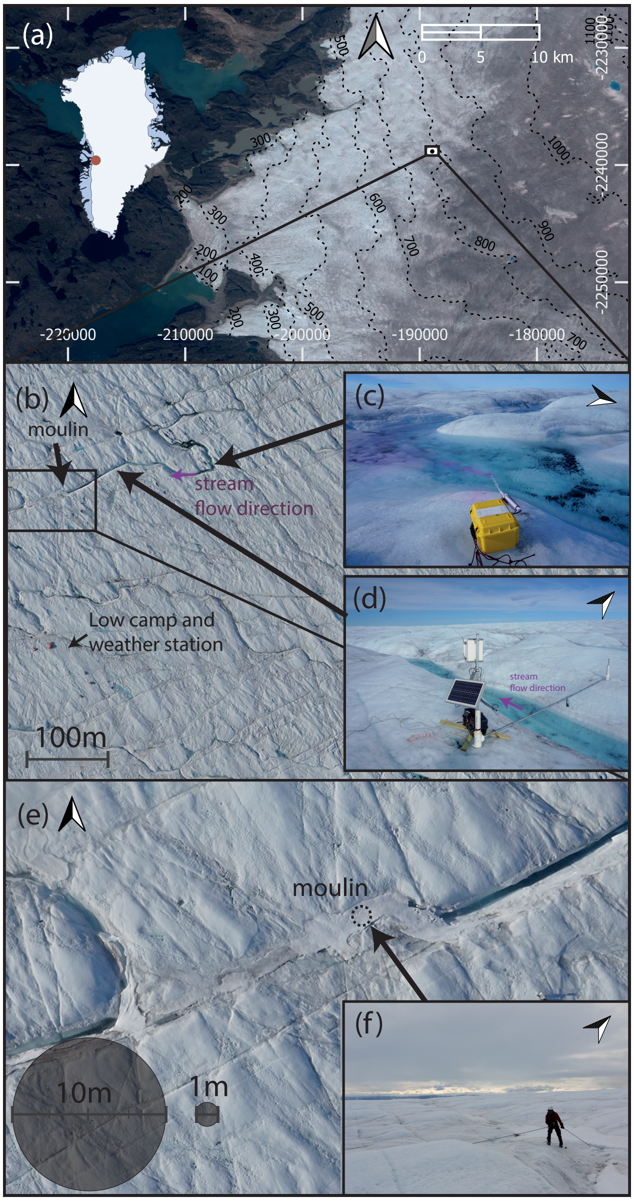

Figure 1. Study site. (a) Sentinel-2 satellite imagery from 2019 of the Pâqitsoq region in Greenland, with coordinates in the EPSG:3413-WGS 84/NSIDC Sea Ice Polar Stereographic North projection, in meters. The field site is indicated with the black box. (b) Orthophoto of the Low Camp field site produced with composite aerial imagery taken with a Tuffwing Uncrewed Aerial Vehicle (UAV) in July 2017. (c) Dye injection site. (d) Stream water level and dye measurement site. (e) Details surrounding the moulin. The arrow indicates the position of the cable where it disappeared under the one-meter wide snow cover on the stream and entered the moulin. (f) Pressure sensor lower in the moulin entrance.

https://doi.org/10.5194/tc-2022-182
Preprint. Discussion started: 20 September 2022

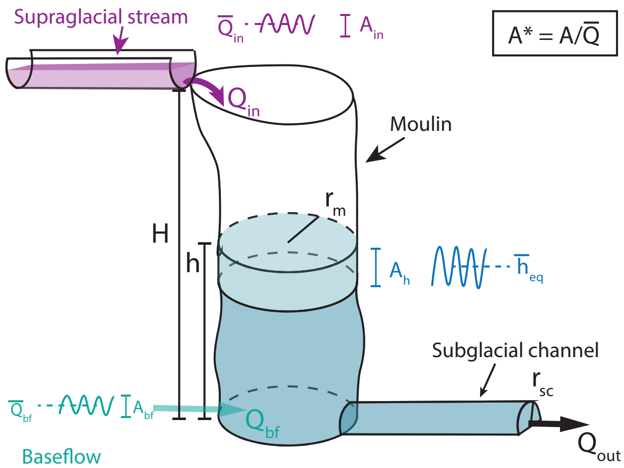

Figure 2. Sketch of the elements of the model, showing water fluxes (Q_{in}, Q_{bf}, Q_{out}), moulin and subglacial channel radii (r_{m}, r_{sc}), ice and water heights (H, h), and fluctuation amplitudes (A_{in}, A_{bf}, A_{h}).

3.1 Meltwater input

We force the model with a modeled and an idealized surface meltwater input (Q_{in}), based on the two days of discharge measurements (Fig. 3d) that we collected upstream of the moulin (Trunz et al., 2021), in order to extend the surface meltwater input timeseries to cover the entire melt season. First, we use a modeled surface input calibrated with the discharge measured in the field. Next, we generalize our stream observations using an idealized sinusoidal surface meltwater input. This sinusoidal forcing has an amplitude of oscillation A_{in} and a mean $\overline{Q}_{\text{in}}$, as shown in Fig. 3.

3.1.1 Measured stream discharge

We measured the discharge ($Q_{\text{in,meas}}$) of the supraglacial stream approximately 100 m upstream of the moulin (Trunz et al., 2021), with a fluorescent dye dilution technique. We injected a Rhodamine WT solution with a peristaltic pump at a rate of $2 \pm 0.5\ \mathrm{mL/min}$ (Q_{pump}). We measured the dye concentration (C_{stream}) with a Turner Cyclops-7 submersible fluorometer calibrated in the field and positioned 100 m downstream of the injection site. We used an injection concentration ($C_{\text{injection}}$) of 200 ppb and calculated the stream discharge using

$$Q_{\text{in,meas}} = C_{\text{injection}} \times Q_{\text{pump}} / C_{\text{stream}} \tag{1}$$

Figure 3 shows the stream flow timeseries obtained over approximately two days. We used this record to calibrate the modeled discharge into the moulin.

https://doi.org/10.5194/tc-2022-182
Preprint. Discussion started: 20 September 2022

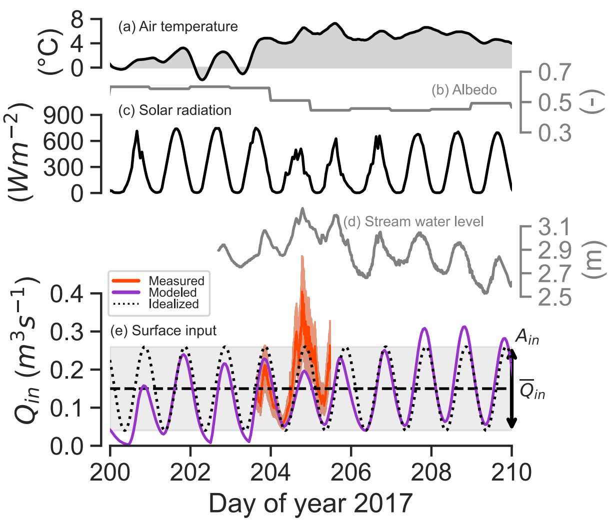

Figure 3. (a–d) Measured weather data used in the melt model from July 1–11, 2017. (e) Surface stream discharge as measured (Sect.3.1.1), modeled (Sect. 3.1.2), and idealized (Sect. 3.1.3) for input into the MouSh model.

3.1.2 Modeled stream discharge

To extend the discharge record beyond the short period of measurement, we modeled the surface melt (M) using an enhanced temperature-index melt model (Pellicciotti et al., 2005) forced with meteorological measurements from a weather station co-located with the moulin (Mejia et al., 2020a).

To more accurately represent surface meltwater input, we add a routing delay to the surface melt timeseries M using a unit hydrograph transfer function, which has previously been utilized for a similar supraglacial stream in Greenland (King, 2018). This is accomplished by convolving the modeled melt with unit hydrograph *UH*:

$$Q_{\text{in,model}} = M * UH, \tag{2}$$

$$UH = \left(\frac{t}{t_{\text{p}}}\right)^{m} \left[e^{m\left(1-\frac{t}{t_p}\right)}\right] Q_{\text{p}} \tag{3}$$

We use the measured 2.5 h time to peak (t_{p}) calculated by Mejia et al. (2022) and empirically set the exponent $m = 1$, which is in the range of values used by King (2018) and Smith et al. (2017) and most accurately reproduces the minimum discharge values at our field area (Fig. 3). We calculate the peak discharge (Q_{p}) as $Q_{\text{p}} = C_{\text{p}}/t_{\text{p}}$, where C_{p} is an empirical coefficient and for which we use the average value of 0.6 from Smith et al. (2017).

We convert measured melt rates (M, $\mathrm{m/s}$) to runoff (R, $\mathrm{m^3/s}$) as follows:

$$R = CMA, \tag{4}$$

where A is the area of the internally drained basin, 0.24 km^2 (Mejia, 2021), and C is a runoff coefficient that we empirically adjust to 0.9 to match the measured diurnal range of the stream discharge (Fig. 3). This runoff coefficient is slightly higher than at the Smith et al. (2017) sites elsewhere in western Greenland, where a range of values from 0.53 to 0.78 was found. This slight discrepancy may be explained by the flatness of our field area, which likely affects the accuracy of our estimate of the drainage basin size A, which would then need to be compensated by an artificial change in C to match the data. Overall, because we used discharge measurements to calibrate the model, we have good confidence in our derived runoff values R and thus our model forcing $Q_{\text{in,model}}$.

We calibrated the melt model by visually comparing its output with the measured stream discharge timeseries. Figure 3 shows the weather data used in the melt model (Fig. 3a–c), the observed stream water level (Fig. 3d), and the three surface meltwater input timeseries (Fig. 3e). A slight discrepancy between measured and modeled stream discharge is apparent on day 205; this is due to a rainfall event not captured by the model. Diurnal stream water level fluctuations (Fig. 3d) are in better agreement with the measured discharge ($R^2 = 0.94$) than with modeled discharge ($R^2 = 0.23$), suggesting that the modeled surface input timeseries is imperfect but still accurately captures most of the observed variability ($p < 0.001$). Therefore, we set m and c to best fit the data on days 204 and 205 to be representative of the overall amplitude of oscillation of the surface input. Note that the surface input model employs only three variables (air temperature, incoming shortwave radiation and albedo); therefore, it does not match all variations in the measured input.

3.1.3 Idealized stream discharge

To separate the effect of diurnal fluctuations of surface input from weekly and seasonal variability, and to simulate a uniformly oscillating baseflow, we define an idealized sinusoidal surface input, Q_{ideal}:

$$Q_{\text{ideal}} = \frac{A}{2}\sin\left(\frac{2\pi(t+\phi)}{P_{\text{osc}}}\right) + \overline{Q}, \tag{5}$$

where A is the peak-to-peak amplitude of oscillation, P_{osc} is the period of oscillation (one day in this set of simulations), t is the time and ϕ is the phase lag, and $\overline{Q}$ is the mean discharge.

For the idealized surface meltwater input $Q_{\text{in,ideal}}$ we assign $A_{\text{in,meas}} = 0.22\ \mathrm{m^3s^{-1}}$ and $\overline{Q}_{\text{in,meas}} = 0.15\ \mathrm{m^3s^{-1}}$ based on the field data shown in Fig. 3. For the subglacial baseflow (Q_{bf}) we vary the amplitude of oscillation (A_{bf}) from 0 to 0.44 $\mathrm{m^3s^{-1}}$ and vary the mean subglacial baseflow ($\overline{Q}_{\text{bf}}$) from 0 to 5 $\mathrm{m^3s^{-1}}$ (Table 2).

3.1.4 Normalized diurnal surface input range

To analyze the effect of supraglacial discharge variability on moulin hydraulic head variations, we introduce a parameter to quantify the relative amplitude of oscillations using a normalized diurnal input range, A^*_{in}:

$$A^*_{\text{in}} = A_{\text{in}} \,/\, \overline{Q_{\text{in}}}, \tag{6}$$

where $\overline{Q}_{\text{in}}$ is the mean supraglacial stream discharge and A_{in} the peak-to-peak amplitude of oscillation.

https://doi.org/10.5194/tc-2022-182
Preprint. Discussion started: 20 September 2022

3.2 Moulin Shape (MouSh) model

To simulate the shape of the moulin and the hydraulic head fluctuations, we use the Moulin Shape (MouSh) model (Andrews et al., 2022). The MouSh model is a two-dimensional physically based model that simulates the depth-dependent size and shape of a moulin for site-specific glacier properties (e.g., ice thickness, ice temperature, external stress, etc.) and for time-varying surface input forcing. The model has five components that enlarge or reduce the moulin radius at each point along a vertical axis, with the ability to melt the upstream and the downstream walls at different rates. These components are illustrated in Fig. 4. The melt components ("turbulence" and "open channel" in the figure) are strongly affected by the surface input rate, while the deformation components ("viscous" and "elastic") are primarily driven by the head, which counteracts the inward ice pressure.

The MouSh model is coupled to a single subglacial channel model (Covington et al., 2020; Trunz et al., 2022) that implements the melting and creep closure equations for a subglacial channel from Schoof (2010). The cross-sectional area of the subglacial channel evolves depending on the hydraulic head and controls the retention and evacuation of the water in the moulin.

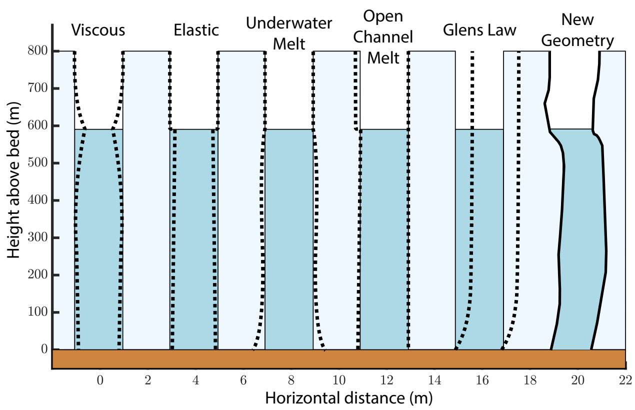

Figure 4. The five components of the MouSh model: deformation (both elastic and viscous), melting (both turbulent underwater and open-channel subaerial), and lateral deformation by Glen's Flow Law. The first four components change the size and shape of the moulin. The final component changes only the shape. Sketch adapted from Andrews et al. (2022).

With realistic combinations of ice thickness and surface input, MouSh predicts head positions consistent with the glacier geometry (i.e., head h between the bed and the ice surface). For certain unusual combinations, MouSh predicts overflowing head, $h > H$, which is unrealistic and rarely observed in the middle of the melt season (an exception being by St Germain and Moorman, 2019, on a high Arctic mountain glacier). Therefore, we set up a threshold in the model that enforces $h \leq H$. Simulations can be run with or without this threshold.

Table 1 lists the values of all constants and tunable parameters we used in all MouSh simulations presented here.

https://doi.org/10.5194/tc-2022-182
Preprint. Discussion started: 20 September 2022

Table 1. Constants and parameters common to all the simulations. The ice temperature profile FOXX 1 is from Lüthi et al. (2015).

Constants	Value	Units
Ice density	910	$\mathrm{kg\,m^{-3}}$
Water density	1000	$\mathrm{kg\,m^{-3}}$
Gravitational acceleration	9.8	$\mathrm{m\,s^{-2}}$
Latent heat of fusion	332000	$\mathrm{J\,kg^{-1}}$
Water dynamic viscosity	$1.7916{\times}10^{3}$	$\mathrm{Pa\,s}$
Water thermal conductivity	0.555	$\mathrm{J\,(m\,K\,s)^{-1}}$
Water heat capacity	4210	$\mathrm{J\,(K\,kg)^{-1}}$
Ice heat capacity	2115	$\mathrm{J\,(K\,kg^{-1}}$
Ice deformation enhancement factor	3	-
Young's modulus	$5{\times}10^{9}$	GPa
Basal ice softness	$6{\times}10^{-24}$	$\mathrm{Pa^{-3}\,s^{-1}}$
Moulin friction factor, f_m	1	-
Subsurface friction factor, f_{oc}	0.5	-
Subglacial friction factor, f_{sc}	0.1	-
Parameters	**Value**	**Units**
Ice thickness, H	500	m
Distance to margin, L	$25{\times}10^{3}$	m
Ice temperature, T	FOXX 1	°C
Regional surface slope, α	0.01	-
Initial moulin radius, $r_m(t=0)$	0.2	m
Initial moulin head, $h(t=0)$	500	m

165 ## 3.3 Simulation categories

To investigate the controls on the observed moulin head oscillations, we test different representations of the englacial and basal hydrologic systems in our model. We compare modeled hydraulic head fluctuations and field observations (Sect. 2) to constrain the possible states of subsurface hydrology, using surface water inputs calculated from field data (Sect. 3.1.2) and constrained by stream discharge measurements (Sect. 3.1.1). In order to constrain how the subglacial drainage system and moulin interact to modify the amplitude of the moulin hydraulic head oscillations, we test different scenarios with fixed cylindrical moulin shapes (0.5 and 5 m radius) or evolving moulin shapes, in both cases with and without additional subglacial water input ("baseflow").

In Table 2 we list all the simulation names and parameters used in this study. We run simulations (Sims) driven by the field-observed stream discharge into a fixed cylindrical moulin (Sim F, for "Fixed") and a shape-evolving moulin (Sim E, for "Evolving"). For the shape-evolving moulin simulations, we run the model without baseflow (Sim EMa) and with baseflow

https://doi.org/10.5194/tc-2022-182
Preprint. Discussion started: 20 September 2022

Table 2. Simulation names and parameters. Parameters are: initial subglacial channel radius ($r_{sc}(t=0)$), moulin radius (r_m), surface input type (Q_{in}), mean surface input ($\overline{Q}_{in}$), peak-to-peak amplitude of surface input (A_{in}), mean baseflow ($\overline{Q}_{bf}$), peak-to-peak amplitude of baseflow (A_{bf}), phase lag (ϕ) between daily peak Q_{in} and peak Q_{bf}. We name the simulation (Sim) according to its broad type: with a fixed (F) or an evolving (E) moulin shape, and whether the surface input is modeled (M) or idealized (I). To specify individual simulations within these broad types, we use lowercase letters (a, b, c, d, e).

	$r_{sc}(t=0)$ shape	r_m (m)	Q_{in} (m^3s^{-1})	$\overline{Q}_{in}$ (m^3s^{-1})	A_{in} (m^3s^{-1})	$\overline{Q}_{bf}$ (m^3s^{-1})	A_{bf} (m^3s^{-1})	ϕ (h)
Sim Fa	0.2	0.5	Modeled	–	–	0	0	0
Sim Fb	0.2	5	Modeled	–	–	0	0	0
Sim Fc	0.2	5	Modeled	–	–	1	0	0
Sim EMa	0.2	Evolving	Modeled	–	–	0	0	0
Sim EMb	0.6	Evolving	Modeled	–	–	2	0	0
Sim EMc	0.6	Evolving	Modeled	–	–	1	0	0
Sim EMd	0.6	Evolving	Modeled	–	–	1	0.2	0
Sim EMe	0.6	Evolving	Modeled	–	–	1	0.2	12
Sim EIa	0.6	Evolving	Idealized	0 to 1	0 to 1	0	0	0
Sim EIb	0.6	Evolving	Idealized	0.15	0.22	0 to 5	0	0
Sim EIc	0.6	Evolving	Idealized	0.15	0.22	0.2, 0.5, 1, 1.5, 2	0.22	0
Sim EId	0.6	Evolving	Idealized	0.15	0.22	1 to 2	0 to 0.44	0, 3, 6, 9, 12

(Sims EMb–e). For the simulations with baseflow, we assign a constant value or allow the baseflow to oscillate diurnally. We performed a wide range of tests and selected two constant baseflow values to present here: a large one of 2 m^3s^{-1} (Sim EMb) and a small one of 0.5 m^3s^{-1} (Sim EMc). For the smaller baseflow value 0.5 m^3s^{-1}, we add an oscillating component with a peak-to-peak amplitude of 0.2 m^3s^{-1} that is either synchronous with the peak meltwater input (Sim EMd), or asynchronous, i.e. with a 12-hour phase lag (Sim EMe). Simulations driven by modeled surface input begin on day 150, which provides a 50-day spin-up period.

Finally, we run three groups of simulations with idealized ("I") surface inputs to explore the modeled response to various (1) surface inputs (Sim EIa), (2) baseflow values (Sim EIb), and (3) surface input and baseflow phase lags (Sims EIc and EId). For each of these simulations with idealized parameter values, we calculate the diurnal range of moulin head variability after a period of ∼23 days. This delay allows moulin head to equilibrate in the more extreme scenarios (Trunz et al., 2022).

https://doi.org/10.5194/tc-2022-182
Preprint. Discussion started: 20 September 2022

The Cryosphere
Discussions
Open Access
EGU

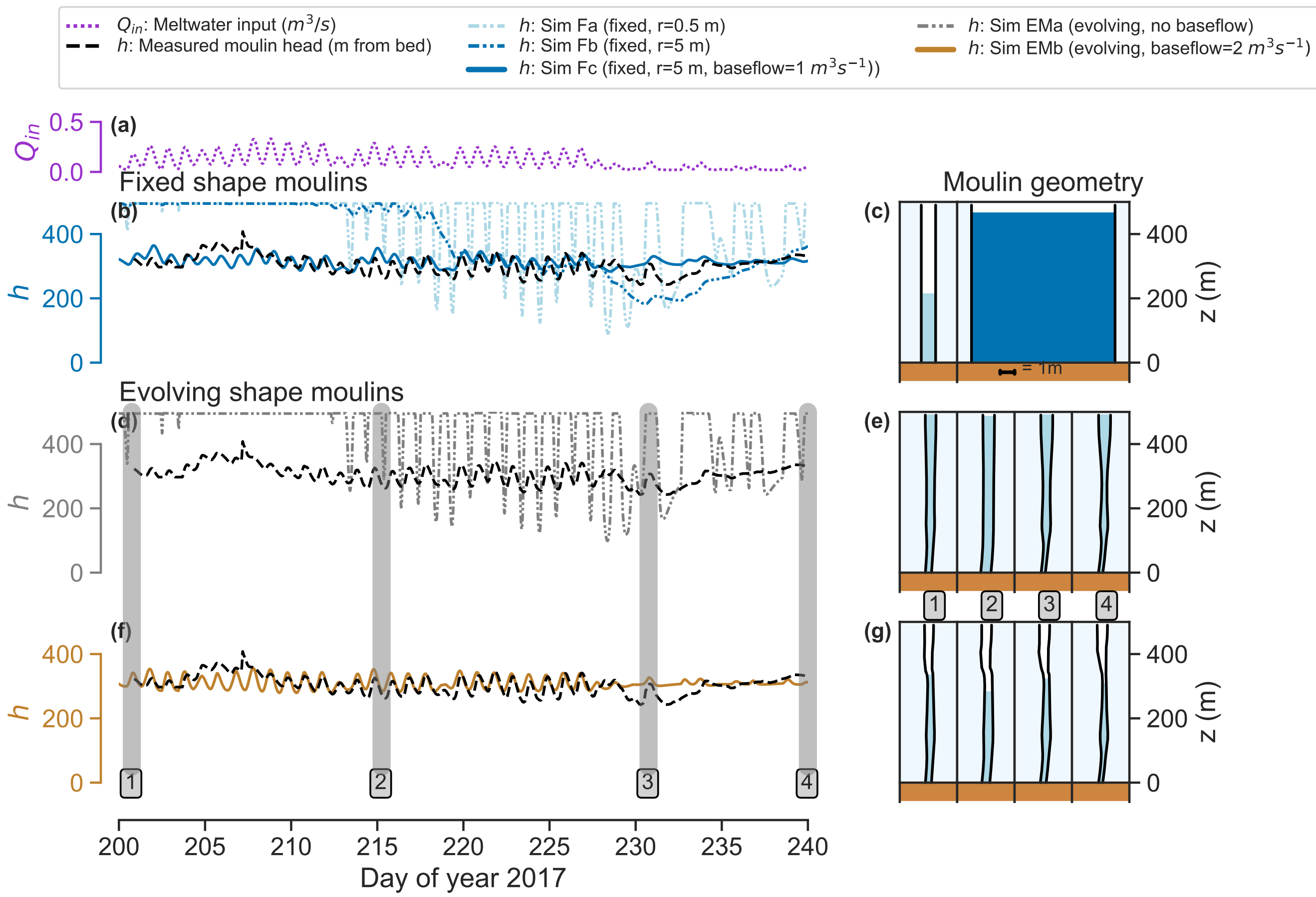

Figure 5. Comparison of three different simulations of moulin hydraulic head and moulin shape for the same (a) surface input stream discharge (Q_{in}) calculated with melt model and scaled with discharge measurements. Simulations Fa, Fb, and Fc: (b–c) Moulin shape is kept fixed with a radius of 0.5 m (left moulin and lighter tone) and 5 m (right moulin and darker tone), with and without baseflow. This simulation illustrates that a large volume is needed to reproduce realistic head amplitude. Simulations EMa: (d–e) Moulin shape evolves with surface input. Simulated head plateaus are caused by head overflowing and model constraints that prevent water from rising higher than the ice thickness. Simulation EMb: (f–g) Moulin shape evolves and an added baseflow reduces the head of oscillation. Panels (c,e,g) show the cross-sectional profile of the moulin. Four different timesteps are numbered and shaded in gray, corresponding to the moulin profiles in panels e and g.

https://doi.org/10.5194/tc-2022-182
Preprint. Discussion started: 20 September 2022

4 Results

4.1 Simulations with realistic inputs

The results of our simulations are shown in Fig. 5. We simulate moulin head with surface inputs (Fig. 5a) calculated using the melt model (Sect. 3). We compare observations for simulations with fixed cylindrical moulins (Fig. 5b–c), evolving moulin shape (Fig. 5d–e), and evolving moulin shape with subglacial baseflow (Fig. 5f–g, and 6).

4.1.1 Fixed moulin shape

The results of the fixed cylindrical shape simulations (Sims Fa–c) are shown in Fig. 5b–d. The fixed cylindrical moulin with the smallest radius (Fig. 1e) of 0.5 m (Fig. 5b–c, lighter blue) produces head oscillations between three and four times the range of moulin head measured in the field. For our model to reproduce measured head oscillations (black lines), a fixed moulin radius of 5 m was required (Fig. 5b, dark blue). Even so, the moulin head oscillations are only within the range of measurements after day 220. Moreover, without baseflow, Sim Fb (the large 5 m moulin) produced a subglacial channel with a cross-sectional area of $\leq$0.3 m^2, which is three orders of magnitude smaller than the $\sim$75 m^2 size of the moulin directly above it. However, the addition of baseflow of $1\mathrm{m}^3\mathrm{s}^{-1}$ (Fig. 5b, dashed dark blue) yields a better reproduction of the head amplitude range measured in the field. In both cases without baseflow, the moulin head sits at the ice sheet surface through the beginning of the melt season, until day 214 (Fig. 5b).

4.1.2 Evolving moulin shape

Next, we show results of simulations where we allow the moulin shape to evolve via viscous deformation, elastic deformation, and wall melt (Sect. 3.2; Sim EMa). These model runs generate a moulin with a radius of ~0.5 m (Fig. 5e), which is comparable to surface observations of the moulin entrance, whose size is constrained by the 1 m width stream. The modeled moulin radius is also highly comparable to the subglacial channel radius of $\sim$1 m (Fig. 6c). However, Sim EMa produces head oscillation amplitudes about six times larger than measured in the field. This large diurnal amplitude causes the simulated head to reach the ice surface ($h = 500$ m) following high surface input events, similar to model runs from fixed-shape moulins with radius of 0.5 m. Head values this high are not supported by our field data.

4.1.3 Effect of baseflow on simulated hydraulic head

We next run simulations with subglacial baseflow (Sims EMb–e). We find that a fixed 2 $\mathrm{m}^3\mathrm{s}^{-1}$ subglacial baseflow (Sim EMb, Fig. 5f–g and Fig. 6b) significantly reduces the amplitude of oscillation of the hydraulic head without changing the order of magnitude of the moulin radius. The moulin radius is generally slightly ($\sim$10 cm) smaller for simulations with baseflow than without. This is because the head stays above overburden pressure for long periods of time in the no-baseflow simulation, decreasing the total amount of viscous and elastic closure.

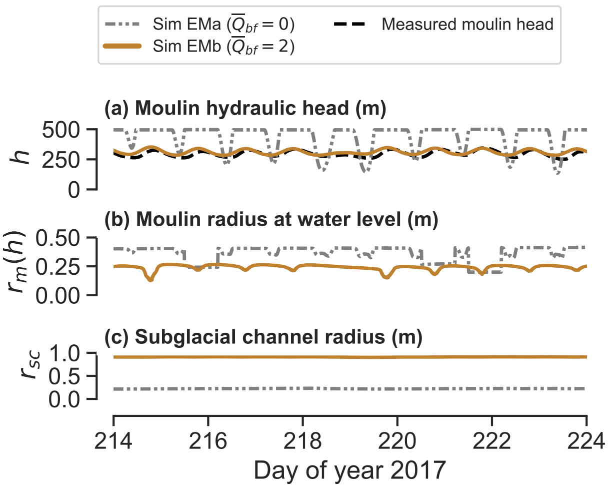

Figure 6. Comparison of (a) moulin hydraulic head, (b) moulin radius, and (c) subglacial radius for simulations with modeled surface input forcing, without subglacial baseflow (Sim EMa, dotted gray) and with 2 $\mathrm{m^3 s^{-1}}$ subglacial baseflow (Sim EMb, solid beige).

While the general diurnal range of moulin head is reproduced, the match between the simulated and measured head is imperfect. We hypothesize three sources for this discrepancy: (1) limitations of the melt model in reproducing particular weather conditions such as cloud coverage, which can underestimate melting, (2) subglacial lake drainages and rain events between days 205 and 210 (Mejia et al., 2021), and (3) the use of a constant value of baseflow, whereas subglacial flow conditions likely evolve throughout the season and enable the moulin water level to decrease at the end of the melt season (example during days 229 to 233).

For a given baseflow magnitude, an oscillating baseflow in phase with the surface meltwater input (Sim EMd) produces larger head oscillation amplitudes than when the baseflow is fixed (Sim EMc; Fig. 7). Additionally, we find that a 12-hour phase lag (Sim EMe) in an oscillating baseflow of 0.5 $\mathrm{m^3 s^{-1}}$ produces a similar head oscillation amplitude as a constant, higher-magnitude (2 $\mathrm{m^3 s^{-1}}$) baseflow (Sim EMb; Fig. 7c).

4.2 Simulations with idealized surface inputs

Here, we investigate the relative effects of surface input (Sim EIa, Fig. 8a), baseflow magnitude (Sim EIb, Fig. 8b), and the phase lag between the baseflow and surface input (Sim EIc, Fig. 8b) on the hydraulic head oscillation dynamics. We use an idealized sinusoidal surface meltwater input and baseflow (Sect. 3) that enables us to control and compare the magnitude and amplitude of oscillations of both the inputs and the simulation outputs.

Figure 8a–b shows our model results without baseflow (Sim EMa) alongside the values of A_h and A^*_in measured for our moulin (Mejia et al., 2021). We plot the mean as a red dot and bars for one standard deviation from the mean. This enables comparison between simulations made with idealized surface inputs and simulations made with the modeled surface inputs

https://doi.org/10.5194/tc-2022-182
Preprint. Discussion started: 20 September 2022

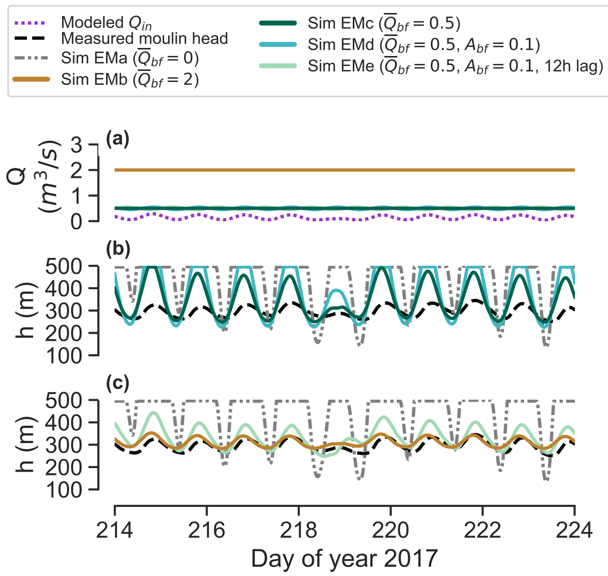

Figure 7. Influence of prescribed baseflow values on modeled moulin hydraulic head. (a) Modeled surface input used for simulations. (b) Moulin hydraulic head simulation for a mean baseflow of 1 $\mathrm{m^3s^{-1}}$, constant and with a peak-to-peak amplitude of oscillation of 0.22 $\mathrm{m^3s^{-1}}$. (c) Moulin hydraulic head amplitude with a constant 2 $\mathrm{m^3s^{-1}}$ and with oscillating 1 $\mathrm{m^3s^{-1}}$ with peak-to-peak amplitude of 0.22 $\mathrm{m^3s^{-1}}$ and a 12-hour phase lag. Measured head is in black and simulated head without baseflow is in dotted gray.

as well as field measurements. To calculate the mean and the standard deviation, we extracted A_h, the measured amplitude of head oscillation, and the modeled oscillation amplitude of the surface input from the simulations EMa and EMb.

In Sim EIb and EIc (Fig. 8b–c) we use a surface input representative of our observations, with a mean discharge of $0.15\ \mathrm{m^3s^{-1}}$ and a peak-to-peak amplitude of $0.22\ \mathrm{m^3s^{-1}}$. The mean measured peak-to-peak head amplitude for the moulin during the middle of the melt season is approximately 10% of the ice thickness, and the mean simulated head with the modeled surface input, without baseflow, and without the ice surface threshold (Sect. 3) is in the range of 60% of the ice thickness.

4.2.1 Effect of normalized diurnal range of surface input on simulated head

First, we investigate how the oscillation amplitude of moulin hydraulic head is affected by the normalized diurnal range of the surface input A^*_in (Sim EIa, Fig. 8a). We simulate the moulin hydraulic head amplitude with selected values of mean surface input and peak-to-peak amplitude ranging from 0 to $1\ \mathrm{m^3s^{-1}}$ (Table 2), and ice thickness of $500\ \mathrm{m}$, the same as we estimate at our field site.

We find that when normalized by the mean discharge, the diurnal range of surface meltwater input strongly influences the simulated relative head amplitude (A_h). Specifically, A_h ranges steadily increase as A^*_in increases from 0 to 0.3. For $A^*_\mathrm{in} > 0.3$, the increase in A_h slows. This is because when the diurnal head range is greater than $\sim 53\%$ of the ice thickness, moulin head reaches the ice surface during diurnal peaks. Because moulin water level cannot exceed the ice thickness, any further

https://doi.org/10.5194/tc-2022-182
Preprint. Discussion started: 20 September 2022

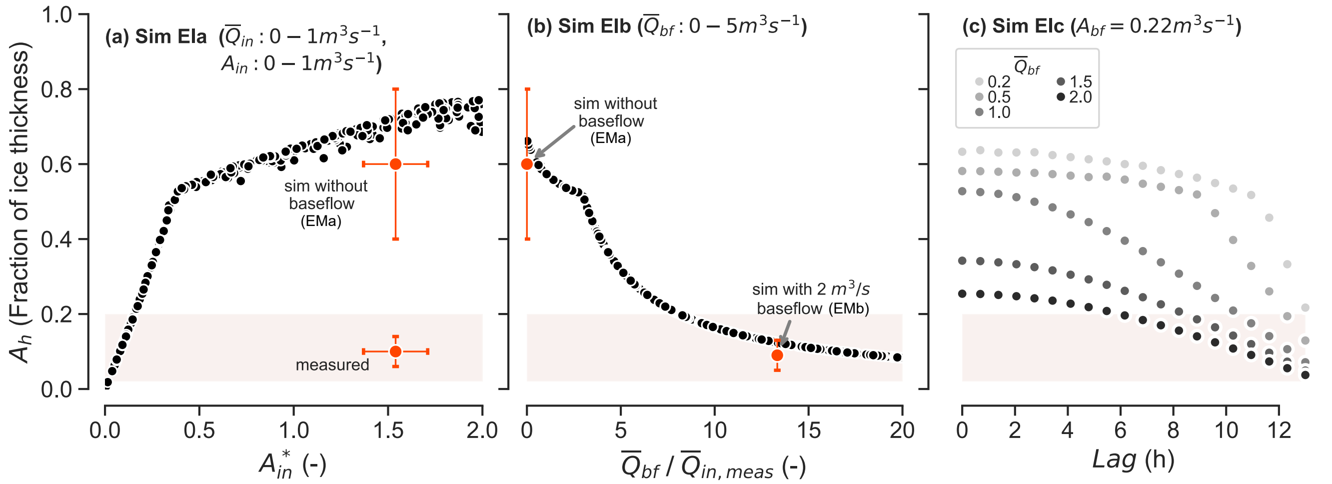

Figure 8. Diurnal range of moulin head (A_h) as a fraction of ice thickness, plotted against (a) normalized diurnal range of the surface input (A^*_in), (b) mean subglacial baseflow ($\overline{Q}_\mathrm{bf}$) divided by the measured mean surface input ($\overline{Q}_\mathrm{in,meas}$), and (c) phase lag between surface input and baseflow. Because the head cannot flow above the ice thickness, head amplitude of oscillation A_h larger than ~53% of the ice thickness are capped, producing a change of slope. (The location of this elbow is dependent on ice thickness; for H=500 m it is A_h ~0.53.) Red dots are values measured in the field or values from simulations with the field based modeled surface inputs, for comparison. Brackets represent variability of one standard deviation from the mean. Red shaded areas represent the field observed range of diurnal range of moulin head.

increases in the amplitude of head oscillations are produced by the lower minimum head values alone. Moulin head oscillates around the equilibrium head, and the distance between the equilibrium head and the ice surface determines the half amplitude of oscillation of the head before it gets capped. Thus, the specific position of the change of slope (elbow in Fig. 8a) depends on the ice thickness and the position of the equilibrium head.

Red dots with one standard deviation error bars in Fig. 8a show the relationship between A^*_in and the A_h for Sim EMa (upper red dot) and that measured in the field (lower red dot). The simulations with modeled surface input (Sim EMa) without baseflow predict a mean hydraulic head diurnal range of 60% of the ice thickness, while field observations show oscillations over just 10% of the ice thickness. Indeed, none of the possible A^*_in scenarios we tested produced A_h results that are consistent with the field measurements.

4.2.2 Effect of constant baseflow on simulated head

Next, we investigate the effect of steady baseflow on the amplitude of diurnal moulin head oscillations (Sim EIb, Fig. 8b). We run simulations with idealized surface input consistent with our field observations (Fig. 3), with a peak-to-peak amplitude of oscillation of 0.22 $\mathrm{m^3s^{-1}}$ and a mean discharge of 0.15 $\mathrm{m^3s^{-1}}$. We find that, in order to reduce the head oscillations into a realistic range (Sim EIb, Fig. 8b), a constant baseflow of at least eight times the mean surface input is required. When the baseflow is less than four times the mean surface input, we observe an unrealistically high head amplitude, and when the

https://doi.org/10.5194/tc-2022-182
Preprint. Discussion started: 20 September 2022

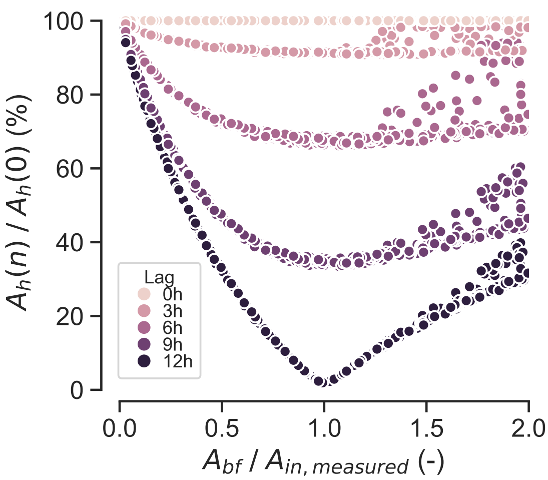

Figure 9. Hydraulic head oscillation amplitude A_h, as a percent of the amplitude without baseflow ($A_h(0)$), versus the ratio between baseflow amplitude (A_{bf}) relative to the measured surface meltwater input amplitude($A_{\mathrm{in,meas}}$), for different surface input–baseflow phase lags. Baseflows with larger amplitudes of oscillations (x-axis), or that are more out of phase with the surface melt (darker colors), generally produce smaller-amplitude head oscillations.

baseflow is higher than six times the mean surface input, the diurnal range of moulin head approaches observed values. To reproduce the observed diurnal range for Sim EMb (Figure 8b, red dot), a constant baseflow of 2 $\mathrm{m^3 s^{-1}}$, which is about fourteen times the mean surface input, is required. Simulation EIb (Fig. 8b) shows that the sensitivity of the diurnal range in head to baseflow magnitude greatly reduces beyond approximately eight times the mean surface input.

4.2.3 Effect of surface input–baseflow phase lag on simulated head

Finally, we investigate the effects of an oscillating baseflow on the time evolution of moulin head. We experiment with different magnitudes and phases of oscillation relative to the surface input Q_{in} (Fig. 8c and Fig. 9). Figure 8c shows the diurnal range in head with a surface input similar to that observed in the field with an oscillating subglacial baseflow with the same amplitude of oscillation (0.22 $\mathrm{m^3 s^{-1}}$) as the surface input. We vary mean subglacial baseflow from 0.2 to 2 $\mathrm{m^3 s^{-1}}$ with a phase lag ranging from 0 to 12-h. With a 12-h phase lag, baseflow values of at least triple the mean surface input are required to dampen moulin head oscillations to match the observed range. On the other hand, with a 6-h phase lag, baseflow fifteen times larger than the mean surface input is required to match observations.

In Figure 9 we investigate the damping of the diurnal head range for five different surface input–baseflow phase lags from 0 to 12 h. The amplitude of moulin head oscillations with a Q_{in}–Q_{bf} phase lag of n hours, $A_h(n)$, is represented in percent of A_h when simulated with zero lag. As baseflow increases, the moulin head oscillation decreases at different rates for different lags, until the amplitude of oscillation of the baseflow, A_{bf}, equals the measured amplitude of oscillation of surface input, $A_{\mathrm{in,meas}}$. When A_{bf} becomes larger than $A_{\mathrm{in,meas}}$, the head oscillation amplitude rises again, at a rate controlled by the amplitude of

https://doi.org/10.5194/tc-2022-182
Preprint. Discussion started: 20 September 2022

The Cryosphere Discussions
Open Access
EGU

Table 3. Normalized diurnal surface input (A^*_{in}) and its constituent properties, mean input ($\overline{Q}_{\text{in}}$) and range of amplitude (A_{in}), observed at supraglacial streams on the Greenland Ice Sheet.

Study	$\overline{Q}_{\text{in}}$ (m^3s^{-1})	A_{in} (m^3s^{-1})	A^*_{in} (–)
Chandler et al. (2013)	~2	~3.5 – 4	1.8 – 2
McGrath et al. (2011)	~0.2	~0.3 – 0.4	1.5 – 2
Marston (1983)	~0.08	~0.1 – 0.16	1.3 – 2
Muthyala et al. (2022)	~0.3	~0.3 – 0.6	1 – 2
Smith et al. (2017)	~15	~15 – 20	1 – 1.3
This study	~0.15	~0.15 – 0.3	1 – 2

baseflow oscillations. Thus, we observe an increase in $A_h(n)$ as $A_{\text{bf}}/A_{\text{in,meas}}$ increases above 1. We also find that when the baseflow and the meltwater amplitude and magnitude are identical ($A_{\text{bf}}/A_{\text{in,meas}}$ = 1) and antiphased (lag of 12 h), the head amplitude drops to zero. As another example, a lag of 6 h with A_{bf} at least half of $A_{\text{in,meas}}$ reduces the moulin head amplitude to 70 % of its value with a zero-lag baseflow.

5 Discussion

In this study, we provide the first comparison of modeled hydraulic head in a shape-evolving moulin to direct field measurements in Greenland. This enables us to scrutinize the relative roles of measured surface meltwater input and hypothesized subglacial water fluxes on a field-observable quantity, moulin head. From this comparison, we infer general traits of regional subglacial connectivity.

We identify three potential controls on the diurnal range of moulin hydraulic head: (1) the normalized diurnal range of the surface meltwater input, (2) the shape of the moulin in the head oscillation range, and (3) the addition of a baseflow. The first control acts as the primary driver of moulin head fluctuations, while the other two are filters that dampen or amplify the surface meltwater input signal (Covington et al., 2020; Trunz et al., 2022). We discuss each of these potential controls in the subsections below.

5.1 Effect of surface input on head oscillation range

Our simulation results in Fig. 8a show that a substantially smaller daily oscillation range of meltwater input ($A^*_{\text{in}} \lesssim 0.2$) than observed in the field is required to produce moulin head oscillations in the measured range. While the snow cover earlier in the melt season might reduce the diurnal variability of A^*_{in}, middle to late melt season measurements of supraglacial discharge elsewhere around Greenland show normalized diurnal range of the surface input A^*_{in} from 1 to 2 (Table 3). This is similar to what we find at our site. The compilation of measurements in Table 3 shows that the daily peak-to-peak oscillation of surface input is usually larger than, and generally at least comparable to, the mean discharge in supraglacial streams entering moulins.

https://doi.org/10.5194/tc-2022-182
Preprint. Discussion started: 20 September 2022

Equivalently, Table 3 shows that surface inputs generally halve ($A^*_{\mathrm{in}} = 1$) and can even drop to near zero ($A^*_{\mathrm{in}} \sim 2$) at their overnight minima.

While moulin size is the dominant control on head oscillation range when considering a wide range of fixed moulin sizes (Covington et al., 2020), we find a clear relationship between the normalized amplitude of input A^*_{in} and the diurnal range of moulin head A_{h} (Fig. 8a) when the moulin size is constrained by a model. Thus, when the moulin shape is known or estimated, the mean discharge through a supraglacial stream ($\overline{Q}_{\mathrm{in}}$), and its diurnal oscillation (A^*_{in}), are central to predicting daily pressure fluctuations.

5.2 Moulin storage as a source of damping

Moulin sizes and shapes in Greenland are poorly constrained by field evidence to date. In our simulations, the radius of the moulin is determined by the MouSh model (Sect. 3.2), which provides an estimate of the moulin size and shape in the portion of the moulin where the water level fluctuates, and allows us to isolate the effect of surface input variability on moulin head oscillation amplitudes (Trunz et al., 2022).

Simulation of moulin head using the field-observed normalized diurnal range of surface input, A^*_{in}, produces extremely large diurnal ranges in head (Sim EMa, Fig. 5d), which overwhelm the model. Similar behavior has been observed in other modeling studies (Cowton et al., 2016; Bartholomew et al., 2012; Werder et al., 2010). Reduction in hydraulic head variability can be obtained by increasing the moulin size, which is inherently uncertain due to limited field exploration to date. For the same surface input forcing, larger moulin volumes will produce more damped oscillations than narrower moulins (Trunz et al., 2022). While large moulin storage volumes may absorb strong variations in surface inputs (Covington et al., 2020; Trunz et al., 2022), for the small-input moulin we study here, the cross-sectional areas would have to be at least ten times larger than predicted by the MouSh model and observed at the surface (Fig. 1e) for this to occur.

5.2.1 Potential upper moulin volume underestimation

In the recent development of the MouSh model (Andrews et al., 2022), results for typical Greenland inputs and ice parameters yielded moulins with radii ~0.5–1 m at the water line, approximately the size of the moulin we study here. Modeled moulins are larger than this above the water line by a factor of ~2–5 (Andrews et al., 2022).

While the mechanisms of shape evolution are better constrained at and below the water line, where the model predicts a moulin cross-sectional area ($\sim 0.3 - 0.5\ \mathrm{m}^2$) of the same order of magnitude as the subglacial channel ($\sim 0.2 - 1\ \mathrm{m}^2$), melt above the water line is complex. MouSh uses a simple parameterization, where melt is controlled by the friction factor, a relatively unconstrained parameter. As a result, we have lower confidence in the accuracy of the modeled volumes in the upper part of the moulin.

Recent field exploration of Greenland moulins discovered cavernous chambers (Covington et al., 2020; Reynaud and Moreau, 1994) where the cross-sectional areas are larger beneath the surface than at the entrance and remain large up to depths of approximately 100 m. The cross-sectional area of the Phobos Moulin (Covington et al., 2020), the largest moulin explored to date, is about ten times larger at a depth of 70 m than it is at the surface. The explored cross-sectional areas deep within

https://doi.org/10.5194/tc-2022-182
Preprint. Discussion started: 20 September 2022

FOXX (Covington et al., 2020) and Isortoq Moulins (Reynaud and Moreau, 1994) are at most about twice the cross-sectional area at the entrances. Thus, large volumes similar to the one present in Phobos Moulin may not be typical of all Greenland moulins. When it was explored in 2018, Phobos had been active for at least two years; in each melt year, the stream feeding it flowed in from a slightly different direction, melting the walls from different sides, which, among other things, could have enlarged the near-surface chamber. Inventories of moulins in this same area suggest that reuse for 2–3 years is common among lake-draining moulins (Poinar and Andrews, 2021; Andrews, 2015), however, the stream typically flows in from a consistent direction. MouSh model runs over a single melt season (Andrews et al., 2022) are able to predict neither this size nor the overhung shape observed in Phobos Moulin.

Thus, there is a distinct possibility that in certain cases, our MouSh results underestimate the volume of the moulin above the water line by a factor of 5–10. The presence of a hypothetical larger upper chamber connected to the water level fluctuation zone in our moulin would reduce the need for baseflow by a factor of three (Sect. 4.1.1) if the volume of the moulin at the water level was ten times larger than the moulin radius at the surface (see comparison of moulin radius in Fig. 1e). However because our instrumented moulin is a recently opened moulin fed by a relatively small stream (Smith et al., 2017), we consider it unlikely that such a large volume would be present 150 m below the surface.

5.2.2 Other sources of englacial or supraglacial storage

Subglacial hydrology models have dealt with extreme head fluctuations produced by the large normalized diurnal range of surface input observed in the field by using larger moulin volumes. On an alpine glacier, Werder et al. (2010) and Schuler and Fischer (2009) both required a moulin radius two to three times larger than they expected in order to damp the simulated head observations. Clarke (1996) used a lumped model with several reservoirs to do the same. Overflowing and overpressurization of the subglacial system is not unique to single-conduit subglacial models. Larger values of englacial void ratios ranging from 1×10^{-4} to 1×10^{-2} (Downs et al., 2018; Hewitt, 2013; Werder et al., 2013) or temporary subsurface storage (Hoffman et al., 2016) are often required in dual distributed–channelized models to prevent overflowing or overpressurization of the subglacial system. Considering a moulin density at our site of 10 moulins per 1 km^2 (Mejia, 2021), and assuming a 1 m moulin radius, we obtain an englacial void ratio of 3×10^{-5}. This is 1–3 orders of magnitude smaller than the values used in the models mentioned above. Hence, moulin storage may not represent the only storage site that allows the damping of subglacial water pressure.

The MouSh model does not account for potential subsurface storage outside the moulin. Such storage has been used to dampen head oscillations in other models via various methods. For example, Bartholomew et al. (2011) use a circular reservoir with a radius 80 times larger than their simulated moulin to temporarily store water and prevent overflow. Cooper et al. (2017) hypothesized the weathering crust as a significant storage reservoir, but we are able to dismiss this possibility for our study area because our measurements of the surface input were taken immediately upstream of where the stream enters the moulin (Fig. 1). As another example, Hoffman et al. (2016) simulated moulin head measured in a similar field area to ours and assumed that when the moulin head was above 60 m below the ice surface, the water was stored in crevasses or fractures that would slowly release it back into the moulin or provide for additional moulin storage in cases where multiple large crevasses intersect each others. In our case, moulin head never reaches this height; at its highest, our measurements show it $\sim$100 m below the surface

(Fig. 5). Crevasses within the field area are unlikely to be sufficiently open to these depths. This is because given the small, centimeter-scale-width of the fractures at the surface, comparing the width:depth aspect ratio of a fracture to the estimated material properties of ice (shear modulus ~ 1 GPa) and surface deviatoric stresses at our field site ($\leq 10 - 100$ kPa), we expect crevasse depth in our area to be around 10 m, but no more than 100 m (Poinar et al., 2017). This rules out significant water storage volumes in crevasses that could intersect the moulin at our location.

5.3 Basal processes as a source of damping

Our model comprises just a single moulin that connects to a single subglacial channel. In reality, multiple moulins within a local area feed a complex subglacial hydrologic network that includes multiple well-connected channels, more isolated areas, and distributed cavities. The model we use does not allow us to simulate those complex processes. However, it gives a first-order estimation of the importance of basal processes in the damping of moulin water level. Accordingly, our addition of baseflow to our model approximates the role of these other systems, especially other moulins and a dendritic channel network.

5.3.1 The requirement for baseflow

Two versions of our simulations produced results that matched field observations: Sims Fb and Fc, a 5 m radius static moulin with and without baseflow, and Sims EMb and EMe, size- and shape-evolving moulins with subglacial baseflow. In the preceding sections, we explored possible scenarios that could produce the englacial storage volumes that would effectively be equivalent to the large moulin in Sim Fb. We found that none of these scenarios were realistic. Here, we explore possible sources of subglacial water flow represented by the baseflow term introduced to our model (see Sims EMb and EMe).

The simulations without baseflow (e.g., Sim EMa) produce a subglacial channel that is too small (0.05 m^2) to have enough discharge capacity to evacuate the water when the head increases at the beginning of each melt day (Fig. 6). This has the result of overfilling the moulin, with the head unrealistically exceeding the ice thickness by midday every day (Fig. 5). Every afternoon, as the discharge in the stream decreases, the water in the moulin is rapidly evacuated through the subglacial channel, which has opened during the day and does not immediately constrict as the surface input reduces. Instead, this closure proceeds overnight under the resulting low moulin head, again producing a small subglacial channel that gets overwhelmed by increasing melt volumes the next morning. We find that increasing the water flux through the subglacial channel makes the water flux in the subglacial channel more constant, preventing the nightly creep closure of the channel. This has the effect of increasing the size and capacity of the subglacial channel, and making it more resilient to diurnal changes in surface input. This increase in water flux is incorporated to our modeled system by the introduction of baseflow to the subglacial channel. Importantly, the inclusion of this baseflow term was the only change or addition to the model that achieved agreement between modeled and observed moulin head.

https://doi.org/10.5194/tc-2022-182
Preprint. Discussion started: 20 September 2022

5.3.2 Subglacial network connectivity and baseflow

Our simulations implement baseflow as a direct addition to the subglacial channel directly upstream of the moulin. This is a first-order modification to our simple, single-channel model that is necessary to make the moulin hydraulic head oscillation agree with field data (Fig. 7). While some moulins may be directly on the path of a subglacial channel and receive significant additional subglacial inputs directly upstream of moulins (Christoffersen et al., 2018; Hoffman et al., 2018; Werder et al., 2013), others initiate the subglacial channel when a crevasse intersects a supraglacial stream (Andrews, 2015; Poinar, 2016; Trunz, 2021). Water exiting moulins that do not feed an existing subglacial flowpath will flow towards a higher-order (larger) subglacial channel (Gulley et al., 2012). Because multiple moulins feed into this higher-order subglacial channel, the discharge within this channel will be larger than what enters our moulin. Thus, this higher-order channel may carry the baseflow that prevents the moulin head from dropping when surface inputs wane, thereby keeping the moulin-connected subglacial channel large enough to readily evacuate the subsequent day's meltwater inputs.

Figure 10 shows a simplified conceptualization of the network connectivity providing the baseflow. Water pressure within the higher-order channel will be controlled by all the moulins feeding it upstream. If the water pressure in the moulin exceeds that in the higher-order channel, water will evacuate the moulin through the tributary. Conversely, if the water pressure in the moulin is lower than in the higher-order channel (for example, when the moulin head is at its nightly low, but the higher-order channel is still in the process of constricting), this will temporarily reverse the hydraulic gradient and provide water input back into the first-order tributary channel, preventing the moulin head from dropping. Overall, the higher-order channel has a stabilizing effect on the head in the tributary and, consequently, in the moulin.

This inference is supported by measurements of normalized diurnal water output ranges at glacier outlets by Bartholomew et al. (2012) and Cowton et al. (2016), which range from 0.1 to 0.5. This is considerably lower than the range in moulins ($A_h \sim 0.4 - 0.8$, Fig. 8), suggesting that diurnal pressure fluctuations in higher-order channels are damped by the network connectivity. Cowton et al. (2016) show that flow in a higher-order channel prevents the head from dropping when surface input decreases. Although they only allow flow in the direction from the moulin to the higher-order channel, their conceptual model would allow the water pressure there to exceed that in the moulin during daily low-input periods in the case of a sustained or lagged higher-order channel discharge. This would be consistent with our concept of temporary flow reversal from the higher-order channel back to the moulin.

5.3.3 Baseflow in the lower and upper ablation zones

Our results show that either a large, constant baseflow or a smaller, oscillating baseflow out of phase with surface input can dampen the diurnal range of moulin head to match field observations. With both the surface input and moulin shape constrained in our modeling setup, we find that a constant subglacial baseflow of 2 $\mathrm{m^3s^{-1}}$, nearly 15 times larger than the mean surface input (Sim EMb), or an antiphased 1 $\mathrm{m^3s^{-1}}$ oscillating baseflow with half the amplitude of oscillation of the surface input (Sim EMe), brings the moulin hydraulic head amplitude of oscillation into the observed range. Which scenario is more likely will vary with location on the ice sheet, as we explain next.

https://doi.org/10.5194/tc-2022-182
Preprint. Discussion started: 20 September 2022

At our study site, we anticipate the discharge in the higher-order subglacial channel connecting to the instrumented moulin to be relatively constant, given the large range of surface input phase lags and magnitudes upglacier from the moulin investigated here (Mejia et al., 2022). We observed at least ten other moulins in a 1 km radius around the moulin in 2017 and 2018 (Mejia, 2021) with relatively small drainage basins (<1 km^2); these all likely feed a common higher-order channel, as we illustrate in Fig. 10. Inputs from nearby moulins with similarly sized drainage basins will increase the discharge in the higher-order subglacial channel and generally stack to produce a daily oscillation in baseflow, similar to Sim EMd. Moulins further upstream, where drainage basins are larger due to thicker ice and lower surface gradients (Yang and Smith, 2016; Andrews et al., 2022), likely also feed this same channel. Input from these moulins, however, will dampen oscillations in the subglacial baseflow by adding out-of-phase discharge to the channel. This would be more consistent with Sim EMb.

Higher on the ice sheet, where the moulin density is much smaller (Phillips et al., 2011; Poinar et al., 2015), we expect a lower water flux through the higher-order subglacial channel, potentially low enough to be more consistent with Sim EMd or Sim EMe (low-flux, oscillating baseflow) than Sim EMb (high-flux, non-oscillating baseflow). If the baseflow oscillation is in phase with the surface input, then it would tend to increase the amplitude of head oscillations (Fig. 7, Sim EMd), whereas field observations suggest that this amplitude actually decreases in thicker ice (Covington, 2020). Thus, we hypothesize that high-elevation moulins are few enough in number that the lag in surface input from one moulin to another should produce the required baseflow oscillations (Sim EMe). This contrasts with low-elevation moulins, whose greater number density and variation in lag should produce a large, minimally oscillating baseflow, similar to Sim EMb.

5.4 Potential external source of baseflow

We speculate and analyze possible origins of the hypothetical baseflow. A recent study shows that fast subglacial water flow velocities recorded with tracer tests require an additional non-local source of subglacial flow (Chandler et al., 2021). This is consistent with our simulation results and with our foremost hypothesis that baseflow originates from the subglacial network connectivity, where moulins are connected to other moulin inputs through an arborescent system of subglacial channels (Davison et al., 2019).

Discrete moulin inputs are necessary for initiating and sustaining efficient subglacial drainage (Dow et al., 2014). While the damping of the hydraulic head for a single moulin can be attributed to its subglacial network connectivity with other moulins, we consider here other potential non-local sources of water.

Previous studies found suggestions of water storage in the englacial and subglacial system (Chu et al., 2016; Poinar et al., 2019; Rennermalm et al., 2013) that could provide a seasonal or year-round water source upstream of our moulin. This could potentially sustain larger subglacial conduits, even for moulins at the upstream edge of the ablation area. In addition, during high water pressure events in moulins, water can be pushed out of the subglacial channel to the surroundings and back to the channel when the pressure in the moulin decreases (Andrews et al., 2014; Mair et al., 2003; Nienow et al., 2005). This could provide for an anti-phased baseflow.

Subglacial meltwater is also produced through basal melting. The geothermal gradient representative of western Greenland is ~50 $\mathrm{mW/m^2}$, which produces basal melt rates of ~5 $\mathrm{cm/a}$ (Fahnestock et al., 2001; Downs et al., 2018). We estimate that

https://doi.org/10.5194/tc-2022-182
Preprint. Discussion started: 20 September 2022

our studied moulin drains an upstream subglacial catchment of ∼2000 km^2, based on subglacial drainage basins calculated by Mankoff (2020); Mankoff et al. (2020) and the local basal melted–frozen boundary estimated by Poinar et al. (2015), which gives a total basal melt flux of ∼3 m^3/s. This is very similar to the subglacial baseflow we require in our simulations (2 m^3/s, Sect. 4.1.3). However, 3 m^3/s is an upper bound because it assumes that all basal melt reaches the subglacial channel system connected to our moulin. In reality, before it can make it to the subglacial channel system, some portion of this available basal melt is stored in the inefficient portion of the drainage system with only a small portion of the water can travel through the linked cavity system (Andrews et al., 2014; Kingslake and Ng, 2013), and some is lost through the bed to the groundwater system (Vidstrand, 2017). At the same time, this will be compensated by surface meltwater inputs from moulins upstream (Sect. 5.3.2). Based on surface melt climatology, we expect the rates of upstream surface water inputs to the higher-order subglacial channels to be larger than the fluxes lost to the inefficient and groundwater systems (Vidstrand, 2017).

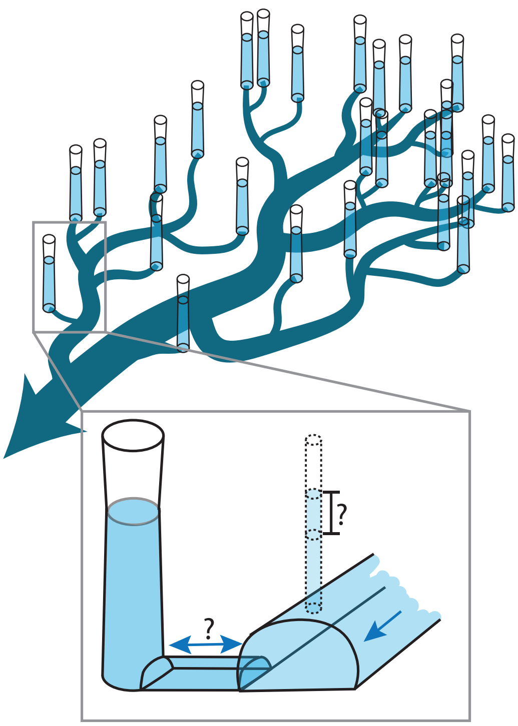

Figure 10. Subglacial network connectivity illustrated by a dendritic subglacial channel system (dark blue), initiated by moulins forming tributaries that connect to higher-order channels.

6 Conclusions

Our results suggest that the moulins on the Greenland Ice Sheet require larger inputs than surface meltwater alone to keep their subglacial channels large enough to accommodate the observed wide diurnal range of surface input. The observed diurnal

https://doi.org/10.5194/tc-2022-182
Preprint. Discussion started: 20 September 2022

range of hydraulic head inside a moulin cannot be explained by local constraints (surface input, moulin size and local ice sheet properties) alone, but requires other, non-local water inputs to the subglacial system. With surface and subsurface external inputs dismissed at our site, this additional water is most likely basal in nature. Local sources of basal water, such as basal melt or groundwater, are unlikely to be large enough to reduce the moulin head amplitude of oscillations. Instead, this requirement for additional subglacial input is best explained by a strong connectivity of the moulin and its subglacial channel to a network of subglacial channels fed by other moulins. This connectivity, or non-local control on moulin hydraulic head and local basal water pressure, suggests a complex subglacial hydraulic network, consistent with other work. Our results provide additional new evidence of the importance of the connectivity of moulins through a subglacial network. Finally, our results suggest that subglacial water flow is lower-magnitude and has stronger daily oscillations at higher altitudes under thicker ice, whereas it is likely steadier at lower altitudes under thinner ice. This difference in subglacial water flux is likely to affect ice motion at higher altitude differently than closer to the margin in future climates, when surface meltwater inputs increase.

Code and data availability. Hydraulic head data for the moulin (called JEME in the dataset) can be found on the Arctic Data Center website at doi:10.18739/A2M03XZ13. Meteorological data used for in the melt model can be found at doi:10.18739/A2CF9J745. Model simulations were produced with the python version of the MouSh model (pyMouSh). The current version of the Github repository containing the pyMouSh model is the Release v.1.0.0 and is available here: https://zenodo.org/record/7058365

Author contributions. CT, KP, and LCA conceived the ideas; CT performed model runs, created the figures, and implemented the unit hydrograph; CT wrote the manuscript with guidance from KP; JM and CT did the data curation; JM implemented the melt model and provided melt timeseries; JM, CT, MDC, VS, and JG designed and coordinated the field effort and collected the field data; MDC and JG acquired funding; All authors reviewed and edited the manuscript.

Competing interests. At least one of the co-authors is a member of the editorial board of *The Cryosphere*. The peer-review process was guided by an independent editor, and the authors also have no other competing interests to declare.

Acknowledgements. C.T., M.D.C., J.M., and J.G. were supported by the United States National Science Foundation grant 1603835. K.P. and L.C.A were supported by NASA Cryosphere grant 80NSSC19K0054. The GNSS base station and on-ice stations were provided by UNAVCO in collaboration with National Science Foundation Logistical support was provided by CH2MHill Polar Services. We thank Charlie Breithaupt, Ronald Knoll, Brandon Conlon and others for their assistance in the field.

References

Andrews, L. C.: Spatial and temporal evolution of the glacial hydrologic system of the western Greenland ice sheet : observational and remote sensing results, Thesis, The University of Texas at Austin, https://doi.org/10.15781/T2WM4V, 2015.

Andrews, L. C., Catania, G. A., Hoffman, M., Gulley, J., Lüthi, M. P., Ryser, C., Hawley, R. L., and Neumann, T. A.: Direct observations of evolving subglacial drainage beneath the Greenland Ice Sheet, Nature, 514, 80–83, https://doi.org/10.1038/nature13796, 2014.

Andrews, L. C., Poinar, K., and Trunz, C.: Controls on Greenland moulin geometry and evolution from the Moulin Shape model, The Cryosphere, 16, 2421–2448, https://doi.org/10.5194/tc-16-2421-2022, 2022.

Badino, G. and Piccini, L.: Englacial water fluctuation in moulins: an example from Tyndall Glacier (Patagonia, Chile), Nimus, pp. 125–129, 2002.

Banwell, A., Willis, I., and Arnold, N.: Modeling subglacial water routing at Paakitsoq, W Greenland, Journal of Geophysical Research: Earth Surface, 118, 1282–1295, https://doi.org/10.1002/jgrf.20093, 2013.

Banwell, A., Hewitt, I., Willis, I., and Arnold, N.: Moulin density controls drainage development beneath the Greenland ice sheet, Journal of Geophysical Research: Earth Surface, 121, 2248–2269, https://doi.org/10.1002/2015JF003801, 2016.

Bartholomew, I., Nienow, P., Sole, A., Mair, D., Cowton, T., King, M., and Palmer, S.: Seasonal variations in Greenland Ice Sheet motion: Inland extent and behaviour at higher elevations, Earth and Planetary Science Letters, 307, 271–278, https://doi.org/10.1016/j.epsl.2011.04.014, 2011.

Bartholomew, I., Nienow, P., Sole, A., Mair, D., Cowton, T., and King, M. A.: Short-term variability in Greenland Ice Sheet motion forced by time-varying meltwater drainage: Implications for the relationship between subglacial drainage system behavior and ice velocity, Journal of Geophysical Research: Earth Surface, 117, F03 002, https://doi.org/10.1029/2011JF002220, 2012.

Catania, G. A. and Neumann, T. A.: Persistent englacial drainage features in the Greenland Ice Sheet, Geophysical Research Letters, 37, L02 501, https://doi.org/10.1029/2009GL041108, 2010.

Chandler, D., Wadham, J. L., Lis, G. P., Cowton, T., Sole, A., Bartholomew, I., Telling, J., Nienow, P., Bagshaw, E. B., Mair, D., Vinen, S., and Hubbard, A.: Evolution of the subglacial drainage system beneath the Greenland Ice Sheet revealed by tracers, Nature Geoscience, 6, 195–198, https://doi.org/10.1038/NGEO1737, 2013.

Chandler, D., Wadham, J. L., Nienow, P. W., Doyle, S. H., Tedstone, A. J., Telling, J., Hawkings, J., Alcock, J. D., Linhoff, B., and Hubbard, A.: Rapid development and persistence of efficient subglacial drainage under 900 m-thick ice in Greenland, Earth and Planetary Science Letters, 566, 116 982, https://doi.org/10.1016/j.epsl.2021.116982, 2021.

Christoffersen, P., Bougamont, M., Hubbard, A., Doyle, S. H., Grigsby, S., and Pettersson, R.: Cascading lake drainage on the Greenland Ice Sheet triggered by tensile shock and fracture, Nature Communications, 9, 1064, https://doi.org/10.1038/s41467-018-03420-8, 2018.

Chu, W., Schroeder, D. M., Seroussi, H., Creyts, T. T., Palmer, S. J., and Bell, R. E.: Extensive winter subglacial water storage beneath the Greenland Ice Sheet, Geophysical Research Letters, 43, 12,484–12,492, https://doi.org/10.1002/2016GL071538, 2016.

Clarke, G. K. C.: Lumped-element analysis of subglacial hydraulic circuits, Journal of Geophysical Research: Solid Earth, 101, 17 547–17 559, https://doi.org/10.1029/96JB01508, 1996.

Cooper, M. G., Smith, L. C., Rennermalm, A. K., Miège, C., Pitcher, L. H., Ryan, J. C., Yang, K., and Cooley, S.: Near surface meltwater storage in low-density bare ice of the Greenland ice sheet ablation zone, The Cryosphere Discussions, pp. 1–25, https://doi.org/10.5194/tc-2017-107, 2017.

Covington, M.: Moulin-volumes-regulate-pressure: code v1.1, https://doi.org/10.5281/zenodo.3987875, 2020.

Covington, M. D., Banwell, A., Gulley, J., Saar, M. O., Willis, I., and Wicks, C. M.: Quantifying the effects of glacier conduit geometry and recharge on proglacial hydrograph form, Journal of Hydrology, 414, 59–71, https://doi.org/10.1016/j.jhydrol.2011.10.027, 2012.

Covington, M. D., Gulley, J. D., Trunz, C., Mejia, J., and Gadd, W.: Moulin Volumes Regulate Subglacial Water Pressure on the Greenland Ice Sheet, Geophysical Research Letters, 47, https://doi.org/10.1029/2020GL088901, 2020.

Cowton, T., Nienow, P., Sole, A., Wadham, J., Lis, G., Bartholomew, I., Mair, D., and Chandler, D.: Evolution of drainage system morphology at a land-terminating Greenlandic outlet glacier, Journal of Geophysical Research: Earth Surface, 118, 29–41, https://doi.org/10.1029/2012JF002540, 2013.

Cowton, T., Nienow, P., Sole, A., Bartholomew, I., and Mair, D.: Variability in ice motion at a land-terminating Greenlandic outlet glacier: the role of channelized and distributed drainage systems, Journal of Glaciology, 62, 451–466, https://doi.org/10.1017/jog.2016.36, 2016.

Davison, B. J., Sole, A. J., Livingstone, S. J., Cowton, T. R., and Nienow, P. W.: The influence of hydrology on the dynamics of land-terminating sectors of the Greenland Ice Sheet, Frontiers in Earth Science, 7, https://doi.org/10.3389/feart.2019.00010, 2019.

de Fleurian, B., Morlighem, M., Seroussi, H., Rignot, E., van den Broeke, M. R., Kuipers Munneke, P., Mouginot, J., Smeets, P. C. J. P., and Tedstone, A. J.: A modeling study of the effect of runoff variability on the effective pressure beneath Russell Glacier, West Greenland, Journal of Geophysical Research: Earth Surface, 121, 2016JF003 842, https://doi.org/10.1002/2016JF003842, 2016.

Dow, C. F., Kulessa, B., Rutt, I. C., Doyle, S. H., and Hubbard, A.: Upper bounds on subglacial channel development for interior regions of the Greenland ice sheet, Journal of Glaciology, 60, 1044–1052, https://doi.org/10.3189/2014JoG14J093, 2014.

Downs, J. Z., Johnson, J. V., Harper, J. T., Meierbachtol, T., and Werder, M. A.: Dynamic Hydraulic Conductivity Reconciles Mismatch Between Modeled and Observed Winter Subglacial Water Pressure, Journal of Geophysical Research: Earth Surface, 123, 818–836, https://doi.org/10.1002/2017JF004522, 2018.

Fahnestock, M., Abdalati, W., Joughin, I., Brozena, J., and Gogineni, P.: High Geothermal Heat Flow, Basal Melt, and the Origin of Rapid Ice Flow in Central Greenland, Science, 294, 2338–2342, https://doi.org/10.1126/science.1065370, 2001.

Flowers, G. E.: Hydrology and the future of the Greenland Ice Sheet, Nature Communications, 9, 2729, https://doi.org/10.1038/s41467-018-05002-0, 2018.

Gulley, J., Benn, D. I., Müller, D., and Luckman, A.: A cut-and-closure origin for englacial conduits in uncrevassed regions of polythermal glaciers, Journal of Glaciology, 55, 66–80, https://doi.org/10.3189/002214309788608930, 2009.

Gulley, J., Walthard, P., Martin, J., Banwell, A., Benn, D., and Catania, G.: Conduit roughness and dye-trace breakthrough curves: why slow velocity and high dispersivity may not reflect flow in distributed systems, Journal of Glaciology, 58, 915–925, https://doi.org/10.3189/2012JoG11J115, 2012.

Hanna, E., Pattyn, F., Navarro, F., Favier, V., Goelzer, H., van den Broeke, M. R., Vizcaino, M., Whitehouse, P. L., Ritz, C., Bulthuis, K., and Smith, B.: Mass balance of the ice sheets and glaciers – Progress since AR5 and challenges, Earth-Science Reviews, 201, 102 976, https://doi.org/10.1016/j.earscirev.2019.102976, 2020.

Hewitt, I.: Seasonal changes in ice sheet motion due to melt water lubrication, Earth and Planetary Science Letters, 371-372, 16–25, https://doi.org/10.1016/j.epsl.2013.04.022, 2013.

Hoffman, M., Andrews, L. C., Price, S. A., Catania, G. A., Neumann, T. A., Luthi, M. P., Gulley, J., Ryser, C., Hawley, R. L., and Morriss, B.: Greenland subglacial drainage evolution regulated by weakly connected regions of the bed, Nature Communications, 7, https://doi.org/10.1038/ncomms13903, 2016.

Hoffman, M., Perego, M., Andrews, L. C., Price, S. F., Neumann, T. A., Johnson, J. V., Catania, G., and Lüthi, M. P.: Widespread Moulin Formation During Supraglacial Lake Drainages in Greenland, Geophysical Research Letters, 45, 778–788, https://doi.org/10.1002/2017GL075659, 2018.

Iken, A.: Measurements of Water Pressure in Moulins as Part of a Movement Study of the White Glacier, Axel Heiberg Island, Northwest Territories, Canada, Journal of Glaciology, 11, 53–58, https://doi.org/10.1017/S0022143000022486, 1972.

Iken, A., Fabri, K., and Funk, M.: Water storage and subglacial drainage conditions inferred from borehole measurements on Gornergletscher, Valais, Switzerland, Journal of Glaciology, 42, 233–248, https://doi.org/10.3189/S0022143000004093, 1996.

King, L. A.: Comparing two methods of remotely estimating moulin discharge on the Greenland ice sheet, Journal of Glaciology, pp. 1–5, https://doi.org/10.1017/jog.2018.65, 2018.

Kingslake, J. and Ng, F.: Modelling the coupling of flood discharge with glacier flow during jökulhlaups, Annals of Glaciology, 54, 25–31, https://doi.org/10.3189/2013AoG63A331, 2013.

Lüthi, M. P., Ryser, C., Andrews, L. C., Catania, G. A., Funk, M., Hawley, R. L., Hoffman, M., and Neumann, T. A.: Heat sources within the Greenland Ice Sheet: dissipation, temperate paleo-firn and cryo-hydrologic warming, The Cryosphere, 9, 245–253, https://doi.org/10.5194/tc-9-245-2015, 2015.

Mair, D., Sharp, M., and C. Willis, I.: Evidence for basal cavity opening from analysis of surface uplift during a high-velocity event: Haut Glacier d'Arolla, Switzerland, Journal of Glaciology, 48, 208–216, https://doi.org/10.3189/172756502781831502, 2002.

Mair, D., Willis, I., Fischer, U. H., Hubbard, B., Nienow, P., and Hubbard, A.: Hydrological controls on patterns of surface, internal and basal motion during three "spring events": Haut Glacier d'Arolla, Switzerland, Journal of Glaciology, 49, 555–567, https://doi.org/10.3189/172756503781830467, 2003.

Mankoff, K.: Streams, Outlets, and Basins [k=1.0], GEUS Dataverse, https://doi.org/10.22008/FK2/XKQVL7, type: dataset version: V2, 2020.

Mankoff, K. D., Ahlstrøm, A. P., Colgan, W., Fausto, R. S., Fettweis, X., Kondo, K., Langley, K., Noël, B., Sugiyama, S., and As, D. v.: Greenland liquid water runoff from 1979 through 2017, Earth System Science Data Discussions, pp. 1–44, https://doi.org/10.5194/essd-2020-47, 2020.

Marston, R. A.: Supraglacial Stream Dynamics on the Juneau Icefield, Annals of the Association of American Geographers, 73, 597–608, https://doi.org/10.1111/j.1467-8306.1983.tb01861.x, 1983.

McGrath, D., Colgan, W., Steffen, K., Lauffenburger, P., and Balog, J.: Assessing the summer water budget of a moulin basin in the Sermeq Avannarleq ablation region, Greenland ice sheet, Journal of Glaciology, 57, 954–964, https://doi.org/10.3189/002214311798043735, 2011.

Meierbachtol, T., Harper, J., and Humphrey, N.: Basal Drainage System Response to Increasing Surface Melt on the Greenland Ice Sheet, Science, 341, 777–779, https://doi.org/10.1126/science.1235905, 2013.

Mejia, J.: Investigating the Hydrology of the Western Greenland Ice Sheet: Spatiotemporal Variability and Implications on Ice-Dynamics, Ph.D. thesis, University of South Florida, Tampa, 2021.

Mejia, J., Trunz, C., Covington, M. D., and Gulley, J.: Meteorological data from two on-ice weather stations at 780 and 950 m asl elevations in the ablation area of Sermeq Avannarleq, West Greenland from 2017-2018, Arctic Data Center, https://doi.org/10.18739/A2CF9J745, type: dataset, 2020a.

Mejia, J., Trunz, C., Covington, M. D., Gulley, J., and Breithaupt, C.: Moulin hydrological measurements from Sermeq Avannarleq, West Greenland Ice Sheet from 2017-2018, Arctic Data Center, https://doi.org/10.18739/A2M03XZ13, type: dataset, 2020b.

Mejia, J., Gulley, J., Trunz, C., Covington, M. D., Bartholomaus, T., Breithaupt, C., Xie, S., and Dixon, T. H.: Moulin density controls the timing of peak pressurization within the Greenland Ice Sheet's subglacial drainage system, https://doi.org/10.1002/essoar.10511864.1, status: submitted to GRL, 2022.

Mejia, J. Z., Gulley, J. D., Trunz, C., Covington, M. D., Bartholomaus, T. C., Xie, S., and Dixon, T. H.: Isolated Cavities Dominate Greenland Ice Sheet Dynamic Response to Lake Drainage, Geophysical Research Letters, 48, e2021GL094 762, https://doi.org/10.1029/2021GL094762, 2021.

Morlighem, M., Williams, C. N., Rignot, E., An, L., Arndt, J. E., Bamber, J. L., Catania, G., Chauché, N., Dowdeswell, J. A., Dorschel, B., Fenty, I., Hogan, K., Howat, I., Hubbard, A., Jakobsson, M., Jordan, T. M., Kjeldsen, K. K., Millan, R., Mayer, L., Mouginot, J., Noël, B. P. Y., O'Cofaigh, C., Palmer, S., Rysgaard, S., Seroussi, H., Siegert, M. J., Slabon, P., Straneo, F., van den Broeke, M. R., Weinrebe, W., Wood, M., and Zinglersen, K. B.: BedMachine v3: Complete Bed Topography and Ocean Bathymetry Mapping of Greenland From Multibeam Echo Sounding Combined With Mass Conservation, Geophysical Research Letters, 44, 11,051–11,061, https://doi.org/10.1002/2017GL074954, 2017.

Muthyala, R., Rennermalm, A. K., Leidman, S. Z., Cooper, M. G., Cooley, S. W., Smith, L. C., and van As, D.: Supraglacial streamflow and meteorological drivers from southwest Greenland, The Cryosphere, 16, 2245–2263, https://doi.org/10.5194/tc-16-2245-2022, https://tc.copernicus.org/articles/16/2245/2022/, 2022.

Nienow, P. W., Hubbard, A. L., Hubbard, B. P., Chandler, D. M., Mair, D. W. F., Sharp, M. J., and Willis, I. C.: Hydrological controls on diurnal ice flow variability in valley glaciers, Journal of Geophysical Research: Earth Surface, 110, https://doi.org/10.1029/2003JF000112, 2005.

Nienow, P. W., Sole, A. J., Slater, D. A., and Cowton, T. R.: Recent Advances in Our Understanding of the Role of Meltwater in the Greenland Ice Sheet System, Current Climate Change Reports, pp. 1–15, https://doi.org/10.1007/s40641-017-0083-9, 2017.

Pellicciotti, F., Brock, B., Strasser, U., Burlando, P., Funk, M., and Corripio, J.: An enhanced temperature-index glacier melt model including the shortwave radiation balance: development and testing for Haut Glacier d'Arolla, Switzerland, Journal of Glaciology, 51, 573–587, https://doi.org/10.3189/172756505781829124, 2005.

Phillips, T., Leyk, S., Rajaram, H., Colgan, W., Abdalati, W., McGrath, D., and Steffen, K.: Modeling moulin distribution on Sermeq Avannarleq glacier using ASTER and WorldView imagery and fuzzy set theory, Remote Sensing of Environment, 115, 2292–2301, https://doi.org/10.1016/j.rse.2011.04.029, 2011.

Pitcher, L. H. and Smith, L. C.: Supraglacial Streams and Rivers, Annual Review of Earth and Planetary Sciences, 47, 421–452, https://doi.org/10.1146/annurev-earth-053018-060212, 2019.

Poinar, K.: The influence of meltwater on the thermal structure and flow of the Greenland Ice Sheet, Ph.D. thesis, University of Washington, https://digital.lib.washington.edu/researchworks/handle/1773/35062, 2016.

Poinar, K. and Andrews, L. C.: Challenges in predicting Greenland supraglacial lake drainages at the regional scale, The Cryosphere, 15, 1455–1483, https://doi.org/10.5194/tc-15-1455-2021, 2021.

Poinar, K., Joughin, I., Das, S. B., Behn, M. D., Lenaerts, J. T. M., and van den Broeke, M. R.: Limits to future expansion of surface-melt-enhanced ice flow into the interior of western Greenland, Geophysical Research Letters, 42, 2015GL063 192, https://doi.org/10.1002/2015GL063192, 2015.

Poinar, K., Joughin, I., Lenaerts, J. T. M., and van den Broeke, M. R.: Englacial latent-heat transfer has limited influence on seaward ice flux in western Greenland, Journal of Glaciology, 63, 1–16, https://doi.org/10.1017/jog.2016.103, 2017.

https://doi.org/10.5194/tc-2022-182
Preprint. Discussion started: 20 September 2022

Poinar, K., Dow, C. F., and Andrews, L. C.: Long-Term Support of an Active Subglacial Hydrologic System in Southeast Greenland by Firn Aquifers, Geophysical Research Letters, 46, 4772–4781, https://doi.org/10.1029/2019GL082786, 2019.

Rennermalm, A. K., Smith, L. C., Chu, V. W., Box, J. E., Forster, R. R., van den Broeke, M. R., Van As, D., and Moustafa, S. E.: Evidence of meltwater retention within the Greenland ice sheet, The Cryosphere, 7, 1433–1445, https://doi.org/10.5194/tc-7-1433-2013, 2013.

Reynaud, L. and Moreau, L.: Moulins glaciaires des glaciers tempérés et froids de 1986 à 1994 (Mer de Glace et Groenland) : morphologie et techniques de mesures de la déformation de la glace, in: Glacier caves and karst in polar regions, Paris, 1994.

Röthlisberger, H.: Water Pressure in Intra- and Subglacial Channels, Journal of Glaciology, 11, 177–203, https://doi.org/10.1017/S0022143000022188, 1972.

Schoof, C.: Ice-sheet acceleration driven by melt supply variability, Nature, 468, 803–806, https://doi.org/10.1038/nature09618, 2010.

Schoof, C., Hewitt, I. J., and Werder, M. A.: Flotation and free surface flow in a model for subglacial drainage. Part 1. Distributed drainage, Journal of Fluid Mechanics, 702, 126–156, https://doi.org/10.1017/jfm.2012.165, 2012.

Schuler, T. V. and Fischer, U. H.: Modeling the diurnal variation of tracer transit velocity through a subglacial channel, Journal of Geophysical Research: Earth Surface, 114, F04 017, https://doi.org/10.1029/2008JF001238, 2009.

Smith, L. C., Chu, V. W., Yang, K., Gleason, C. J., Pitcher, L. H., Rennermalm, A. K., Legleiter, C. J., Behar, A. E., Overstreet, B. T., Moustafa, S. E., Tedesco, M., Forster, R. R., LeWinter, A. L., Finnegan, D. C., Sheng, Y., and Balog, J.: Efficient meltwater drainage through supraglacial streams and rivers on the southwest Greenland ice sheet, PNAS, 112, 1001–1006, https://doi.org/10.1073/pnas.1413024112, 2015.

Smith, L. C., Yang, K., Pitcher, L., Overstreet, B., Chu, V., Rennermalm, A., Ryan, J., Cooper, M., Gleason, C., Tedesco, M., Jeyaratnam, J., van As, D., van den Broeke, M. R., van de Berg, W. J., Noël, B., Langen, P., Cullather, R., Zhao, B., Willis, M., Hubbard, A., Box, J., Jenner, B., and Behar, A.: Direct measurements of meltwater runoff on the Greenland ice sheet surface, PNAS, 114, E10 622–E10 631, https://doi.org/10.1073/pnas.1707743114, 2017.

Sommers, A., Rajaram, H., and Morlighem, M.: SHAKTI Subglacial Hydrology and Kinetic, Transient Interactions v1.0, Geoscientific Model Development, 11, 2955–2974, https://doi.org/10.5194/gmd-11-2955-2018, 2018.

Spring, U. and Hutter, K.: Numerical studies of jökulhlaups, Cold Regions Science and Technology, 4, 227–244, 1981.

St Germain, S. L. and Moorman, B. J.: Long-term observations of supraglacial streams on an Arctic glacier, Journal of Glaciology, 65, 900–911, https://doi.org/10.1017/jog.2019.60, 2019.

Trunz, C.: Modeling and Measuring Water Level Fluctuations in the Greenland Ice Sheet: How Moulin Life Cycle and Shape can Inform us on the Subglacial Drainage System., Doctoral Thesis, University of Arkansas, Fayetteville, 2021.

Trunz, C., Mejia, J., Covington, M., Siegel, V., Conlon, B., and Gulley, J.: Supraglacial stream discharge measurements from six catchments within the Pâqitsoq region of Sermeq Avannarleq, western Greenland Ice Sheet 2017 -2018, Arctic Data Center, https://doi.org/10.18739/A2D21RK53, type: dataset, 2021.

Trunz, C., Covington, M. D., Poinar, K., Andrews, L. C., Mejia Zimmerman, J., and Gulley, J.: Modeling the influence of moulin shape on subglacial hydrology, Journal of Geophysical Research: Earth Surface, status: accepted, 2022.

Vidstrand, P.: Concept testing and site-scale groundwater flow modelling of the ice sheet marginal-area of the Kangerlussuaq region, Western Greenland, Tech. Rep. R-15-01, SVENSK KÄRNBRÄNSLEHANTERING AB, Solna, http://www.skb.se/publikation/2488544/R-15-01.pdf, 2017.

Walder, J. S.: Hydraulics of Subglacial Cavities, Journal of Glaciology, 32, 439–445, https://doi.org/10.3189/S0022143000012156, 1986.

https://doi.org/10.5194/tc-2022-182
Preprint. Discussion started: 20 September 2022

Werder, M. A., Schuler, T. V., and Funk, M.: Short term variations of tracer transit speed on alpine glaciers, The Cryosphere, 4, 381–396, https://doi.org/10.5194/tc-4-381-2010, 2010.

Werder, M. A., Hewitt, I. J., Schoof, C., and Flowers, G. E.: Modeling channelized and distributed subglacial drainage in two dimensions, Journal of Geophysical Research: Earth Surface, 118, 2140–2158, https://doi.org/10.1002/jgrf.20146, 2013.

Willis, I. C.: Intra-annual variations in glacier motion: a review, Progress in Physical Geography, 19, 61–106, https://doi.org/10.1177/030913339501900104, 1995.

Yang, K. and Smith, L. C.: Internally drained catchments dominate supraglacial hydrology of the southwest Greenland Ice Sheet, Journal of Geophysical Research: Earth Surface, 121, 2016JF003 927, https://doi.org/10.1002/2016JF003927, 2016.